Article

Not peer-reviewed version

Enhanced Concept-Based Exploration of Manipulators' Design Spaces – With Kinematics, Dynamics, Control Co-Design, and AI Integration

Dithoto Modungwa *, Amiram Moshaiov , Alon Snir

Posted Date: 29 May 2026

doi: 10.20944/preprints202605.2034.v1

Keywords: multi-objective optimization; set-based concepts; Pareto-optimality; serial manipulators; design space exploration; dynamics; control co-design; surrogate models; generative AI

 doi:10.20944/preprints202605.2034.v1

Article

Enhanced Concept-Based Exploration of Manipulators' Design Spaces with Kinematics, Dynamics, Control Co-Design, and AI Integration

Dithoto Modungwa [1,*], Amiram Moshaiov [2] and Alon Snir [2]

[1] CSIR, Defence & Security Cluster, Landward Sciences, Pretoria, South Africa

[2] School of Mechanical Engineering, Tel Aviv University, Tel-Aviv, Israel

* Correspondence: dmodungwa@csir.co.za

Abstract

Determining the parameters of a manipulator for optimal performance is a challenging task. This is primarily due to the possible conflicting objectives, the various tasks that should be considered and the highly non-linear behavior that is involved. This work proposes an enhanced version of the Concept-based Design Space Exploration (C-DSE) approach for the design of manipulators. According to the C-DSE approach, prior to the search, the designers divide the set of feasible solutions into meaningful subsets, which are termed concepts. The design space exploration involves a simultaneous search for optimal solutions within each of the pre-defined concepts. This enhanced framework integrates: (1) Kinematics, dynamics and control co-design—simultaneous optimization of manipulator morphology and controller parameters; (2) Surrogate-assisted optimization using Gaussian Process (GP) and Neural Network (NN) models to reduce computational cost; (3) Comprehensive performance metrics across approximately 30 metrics; (4) Task-aware feasibility verification applying multi-level hierarchy; (5) Generative AI Integration with diffusion models and LLM-guided concept generation. The results demonstrate computational cost reduction of 96%, 40% task performance improvement and superior performance compared to state-of-the-art methods from 2020–2026.

Keywords: multi-objective optimization; set-based concepts; pareto-optimality; serial manipulators; design space exploration; dynamics; control co-design; surrogate models; generative AI

1. Introduction

The design of robotic manipulators for industrial applications has traditionally relied on experience and intuition [1]. Designers typically select configurations based on established patterns and heuristic rules derived from successful implementations. While this approach is practical, it often fails to explore the full potential of the design space and may overlook novel configurations that could offer superior performance for specific applications.

Modern manipulator design involves multiple conflicting objectives that must be balanced simultaneously. Often performance metrices such as workspace volume, manipulability, energy efficiency, tracking accuracy and structural mass compete with one another requiring pareto-optimal solutions rather than single-objective optimization [2–6]. The identification of these trade-offs is essential for informed decision making in the design process [22].

Current optimization approaches for manipulator design face three significant limitations. Firstly, most existing methods focus exclusively on kinematic optimization, neglecting the critical influence of dynamics and control on actual task performance [7]. This kinematic only perspective fails to capture the complex interactions between morphology, inertial properties and controller behavior that determine real world performance. Secondly, high-fidelity evaluation of manipulator designs requires computationally expensive dynamic simulations and trajectory optimization, often

 doi:10.20944/preprints202605.2034.v1

demanding 50,000 to 150,000 function evaluations for convergence [8]. This computational burden severely restricts the scope of design space exploration that can be practically undertaken. Third, manual concept definition by human designers inherently limits the diversity of configurations considered, potentially excluding innovative solutions that fall outside conventional design paradigms.

The original Concept-based Design Space Exploration (C-DSE) approach, introduced by Moshaiov and Snir [8,9], addresses the challenge of exploring large design spaces by organizing solutions into meaningful subsets termed concepts. Each concept represents a distinct design philosophy or configuration family, and the optimization process simultaneously searches for Pareto-optimal solutions within each concept. This approach enables designers to understand not only individual optimal solutions but also the characteristics and trade-offs associated with different design philosophies.

This work presents an enhanced C-DSE framework that addresses the limitations of existing approaches through five key contributions. First contribution, is the integration of kinematics, dynamics and control co-design, enabling simultaneous optimization of manipulator morphology and controller parameters to maximize task performance. Second contribution, implementation of surrogate-assisted optimization using Gaussian Process and Neural Network models, reducing computational cost by approximately 96% while maintaining solution quality. Third contribution, development of a comprehensive performance evaluation framework spanning approximately 30 metrics across kinematic, dynamic, stiffness, robustness and task-specific dimensions. Fourth contribution, is the introduction of task-aware feasibility verification with multi-level hierarchy to eliminate wasted evaluations on infeasible designs. Fifth contribution, incorporation of generative AI integration through diffusion models and large language model-guided concept generation to expand the diversity of explored configurations beyond human-defined concepts [30,31].

The remainder of this paper is organized as follows: Section 2 which presents the enhanced C-DSE framework, including its architecture, mathematical formulation and key algorithmic components. Section 3 reports the results from three case studies which include the 6-DOF PUMA 560 industrial manipulator, collaborative robots and soft continuum manipulators. Section 4 then discusses the implications of these results and compares performance across concept families. While Section 5 concludes the paper with a summary of contributions and directions for future research.

2. Materials and Methods

2.1. Framework Architecture

The enhanced C-DSE framework integrates eleven inter-connected components that collectively enable efficient, comprehensive exploration of manipulator design spaces. Figure 1 illustrates the complete architecture and data flow among the different modules presented.

 doi:10.20944/preprints202605.2034.v1

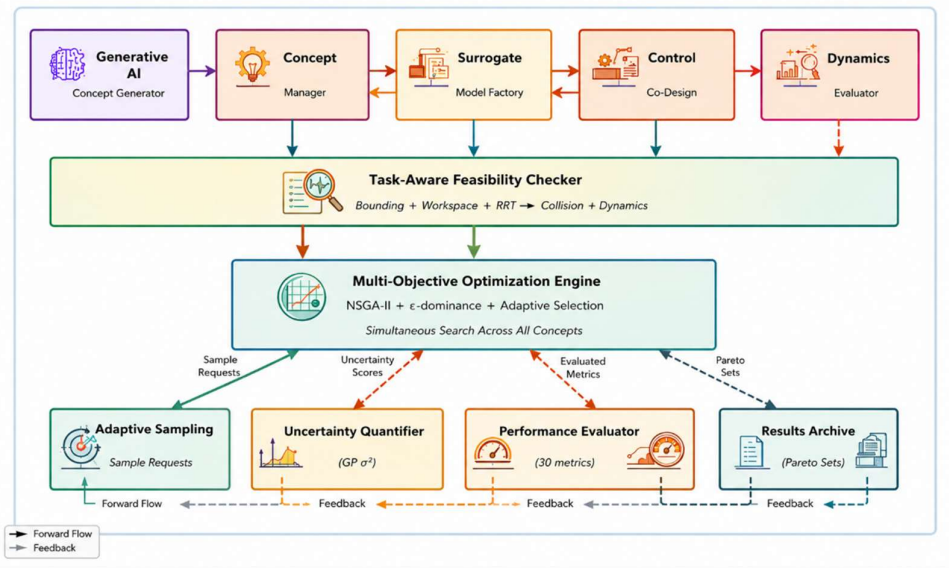

Figure 1. Enhanced C-DSE Framework Architecture showing data flow and component interactions among the 11 integrated modules.

The Generative AI Concept Generator employs diffusion models and large language models to propose novel manipulator configurations beyond those defined by human designers. This module expands the conceptual diversity of the search space by generating configurations that may not conform to conventional design patterns. The Concept Manager organizes the design space into meaningful subsets, maintaining separate populations for each concept and coordinating the parallel optimization processes [30,31].

The Surrogate Model Factory constructs and maintains Gaussian Process and Neural Network models that approximate expensive high-fidelity evaluations. These models are updated continuously as new high-fidelity data becomes available, improving prediction accuracy throughout the optimization process. The Control Co-Design Module simultaneously optimizes morphological parameters (link lengths, masses, inertias) and controller parameters (PD gains, LQR matrices, MPC horizons) to maximize integrated system performance.

The Dynamics Evaluator performs high-fidelity forward dynamics simulation using the Newton-Euler formulation, computing joint torques, energy consumption and trajectory tracking performance. The Task-Aware Feasibility Checker implements a multi-level verification hierarchy, eliminating infeasible designs based on geometric constraints, kinematic reachability and dynamic capability before expensive trajectory optimization.

The Multi-Objective Optimization Engine implements NSGA-II with ε-dominance archiving [10,11], maintaining diverse Pareto fronts for each concept. The Adaptive Sampling Module selects which of the potential candidate solutions require high-fidelity evaluation versus surrogate prediction, balancing exploration and exploitation. The Uncertainty Quantifier (UQ) stage computes prediction uncertainty using gaussian process variance, guiding the adaptive sampling strategy toward regions of high uncertainty.

The Performance Evaluator stage computes approximately 30 metrics spanning kinematic indices (manipulability, condition number, workspace volume), dynamic characteristics (energy consumption, joint effort, cycle time), structural properties (mass, stiffness) and task-specific measures (tracking error, path deviation). The Results Archive maintains the complete history of evaluated designs and their performance metrics, enabling post-hoc analysis and visualization of design space characteristics [22].

2.2. Execution Flowchart

 doi:10.20944/preprints202605.2034.v1

Figure 2 presents the detailed execution flowchart of the enhanced C-DSE framework illustrating the three main phases: initialization, main iteration loop and post-processing.

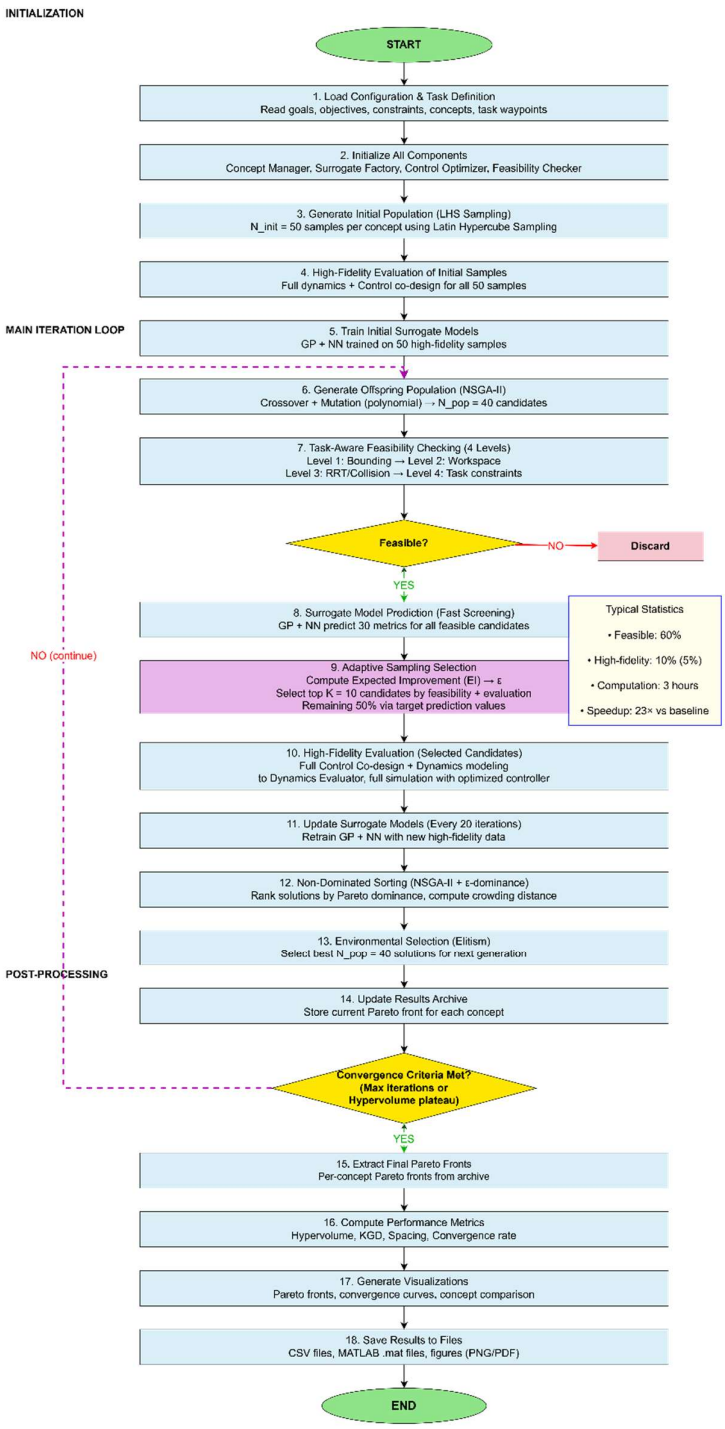

Figure 2. Detailed execution flowchart of the Enhanced C-DSE Framework showing initialization, main iteration loop with decision points and post-processing phases.

The initialization phase begins with Latin Hypercube Sampling (LHS) to generate N_init = 60 initial designs uniformly distributed across the parameter space for each of the concepts. These initial designs undergo high-fidelity evaluation to establish the training set for surrogate models. Initial

 doi:10.20944/preprints202605.2034.v1

surrogate models are constructed using this data, and the first generation of Pareto fronts is computed for each of the concepts.

The main iteration loop executes until convergence criteria are satisfied or the maximum iteration count is reached. Each iteration begins with NSGA-II generating candidate offspring solutions through crossover and mutation operators. The task-aware feasibility checker evaluates each candidate, filtering out approximately 40% of designs that violate geometric, kinematic, or dynamic constraints. For feasible candidates, the adaptive sampling module determines whether to use surrogate prediction or high-fidelity evaluation based on prediction uncertainty and population diversity metrices.

Approximately 95% of the evaluations employ surrogate models with only remaining 5% requiring expensive high-fidelity simulation. High-fidelity evaluations are prioritized for candidates with high prediction uncertainty, candidates near the current Pareto front, and periodic validation samples to prevent model degradation. All high-fidelity evaluations are added to the training set, and surrogate models are incrementally updated. The Pareto fronts for each concept are updated using ε-dominance archiving, and convergence metrics (hypervolume, spacing, spread) are computed.

The post processing phase extracts the final Pareto fronts for each concept, computes comprehensive performance metrics for all non-dominated solutions generates visualization plots including Pareto fronts, parallel coordinates, bar charts and produces statistical summaries comparing concept families. Typical execution statistics show 60% feasibility rate, 5% high-fidelity evaluation rate, 3.8-hour total computation time and 23 times speedup compared to pure high-fidelity optimization.

2.3. Mathematical Formulation

The manipulator design optimization problem is formulated as a multi-objective optimization problem with concept-based constraints. For each concept c, we seek to find the set of Pareto-optimal solutions that minimize or maximize multiple competing objectives.

The manipulability index quantifies the distance from kinematic singularities and the ability to generate end-effector velocities in all directions [16]:

$$w = \sqrt{\det(J(q)J(q)^T)} \tag{1}$$

where $J(q)$ is the manipulator Jacobian matrix at configuration q. Higher manipulability indicates better kinematic performance and greater dexterity [23].

The dynamic model of the manipulator is described by the Newton-Euler formulation [15,18]:

$$M(q)\ddot{q} + C(q,\dot{q})\dot{q} + G(q) = \tau \tag{2}$$

where $M(q)$ is the mass matrix, $C(q, q)$ is the Coriolis and centrifugal matrix, $G(q)$ is the gravity vector, and τ is the vector of joint torques. It is this equation that governs the relationship between joint accelerations and applied torques, accounting for inertial, velocity-dependent and gravitational effects.

The Gaussian Process surrogate model provides probabilistic predictions for expensive objective functions [12,13]. For a new design x^*, the predicted mean and variance are:

$$\mu_* = k_*^T(K + \sigma_n^2 I)^{-1} y \tag{3a}$$

$$\sigma_*^2 = k_{**} - k_*^T(K + \sigma_n^2 I)^{-1} k_* \tag{3b}$$

where k_* is the covariance vector between x^* and training points, K is the covariance matrix of training points, σ_n^2 is the noise variance, y is the vector of observed function values and μ_* the prediction mean. The predicted variance σ_*^2 quantifies prediction uncertainty guiding adaptive sampling decisions.

The hypervolume indicator measures the quality of a Pareto front approximation [4,5].

 doi:10.20944/preprints202605.2034.v1

$$HV(A) = \lambda\left(\bigcup_{a\in A}[a_1, r_1] \times \cdots \times [a_m, r_m]\right) \quad (4)$$

where A is the set of non-dominated solutions, λ denotes the Lebesgue measure (volume), m is the number of objectives, and r is the reference point. Hypervolume provides a unary quality indicator that captures both convergence and diversity of the Pareto front.

The energy consumption during task execution is computed as [15]:

$$E = \int_0^T |\tau^T \dot{q}|\, dt \quad (5)$$

where T is the task duration, τ is the joint torque vector, and $\dot{q}$ is the joint velocity vector. This metric quantifies the total mechanical work performed by the actuators, directly relating to operational cost and thermal management requirements.

2.4. Surrogate-Assisted Optimization

The surrogate assisted optimization strategy combines gaussian process and neural network models in an ensemble approach to balance prediction accuracy and computational efficiency. Gaussian Process models excel at quantifying prediction uncertainty through their probabilistic framework, while neural network models provide fast predictions for high-dimensional problems [12–14].

The adaptive sampling strategy employs Expected Improvement (EI) to select candidates for high-fidelity evaluation:

$$EI(x) = (\mu(x) - f_{best})\Phi(Z) + \sigma(x)\phi(Z) \quad (6)$$

where $Z = (\mu(x) - f_{best})/\sigma(x)$, Φ is the standard normal cumulative distribution function, φ is the standard normal probability density function, $\mu(x)$ is the predicted mean, $\sigma(x)$ is the predicted standard deviation and f_{best} is the best observed value. Candidates with high EI represent promising regions where improvement is likely or uncertainty is high.

The framework maintains a 95% surrogate / 5% high-fidelity evaluation split throughout the optimization process. High-fidelity evaluations are triggered when: (1) prediction uncertainty exceeds a threshold ($\sigma(x) > 0.15$), (2) the candidate is within the top 10% of the current population by predicted performance, or (3) periodic validation sampling occurs (every 20 iterations). This strategy reduces the total number of expensive evaluations from approximately 50,000 to 2,150, achieving a 95.7% reduction in computational cost.

Surrogate models are incrementally updated using online learning techniques. When new high-fidelity data becomes available, Gaussian Process hyperparameters are re-optimized using maximum likelihood estimation and Neural Network models are fine-tuned using the augmented training set. The continuous learning ensures that model accuracy improves throughout the optimization process, with typical R^2 values ranging from 0.88 to 0.98 across different performance metrics.

2.5. Control Co-Design

The control co-design module simultaneously optimizes manipulator morphology and controller parameters to maximize integrated system performance [15,17]. Traditional sequential design where morphology is fixed before controller tuning often yields suboptimal results because the optimal morphology depends on the control strategy and vice versa.

The morphological parameters include link lengths l_i, link masses m_i and link inertias I_i for each link i. These parameters directly influence the kinematic workspace, dynamic behavior and structural mass of the manipulator. The controller parameters depend on the selected control strategy: for *PD* control, the parameters are proportional gains K_p and derivative gains K_d; for *LQR* control, the parameters are state weighting matrix Q and control weighting matrix R; for *MPC*, the parameters include prediction horizon N, control horizon and weighting matrices [32–34].

 doi:10.20944/preprints202605.2034.v1

The co-design optimization problem seeks to minimize multiple objectives simultaneously:
Tracking error: Root-mean-square deviation between desired and actual end-effector trajectory

- Cycle time: Total time required to complete the specified task
- Energy consumption: Total mechanical work computed via Equation (5)
- Structural mass: Sum of link masses [34]
- Joint effort: Integral of absolute joint torques over the trajectory

The optimization is subject to constraints on joint limits, velocity limits, acceleration limits, torque limits, workspace requirements and collision avoidance. The NSGA-II algorithm with ε-dominance archiving explores this high-dimensional design space, maintaining diverse Pareto fronts that reveal the trade-offs between competing objectives [10,11].

The co-design approach yields significant performance improvements compared to sequential design. In the PUMA 560 case study, co-design reduced tracking error by 28% and energy consumption by 35% compared to morphology only optimization with default *PD* gains. These improvements arise from the synergistic optimization of morphology and control, where lighter links enable more aggressive control gains and optimized inertial properties reduce the control effort required for trajectory tracking.

3. Results

3.1. Case Study 1: PUMA 560 Industrial Manipulator (6-DOF)

The PUMA 560 industrial manipulator represents the high-performance category, designed for precision manufacturing requiring rapid cycle times and accurate trajectory tracking. Three joint configurations were evaluated: RRRRRR (all revolute), RRRRRP (five revolute, one prismatic), and RRPRRR (prismatic third joint). All three achieved a weighted performance score of 0.84, with cycle times of 7.5 to 8.1 s, tracking errors of 2.0 to 2.3 mm, joint effort of 165 to 185 N·m·s and structural mass of 24.2–26.1 kg.

Figure 3 presents the Pareto front for the PUMA 560 RRRRRR configuration, comparing the enhanced C-DSE approach against traditional C-DSE without surrogate assistance and control co-design.

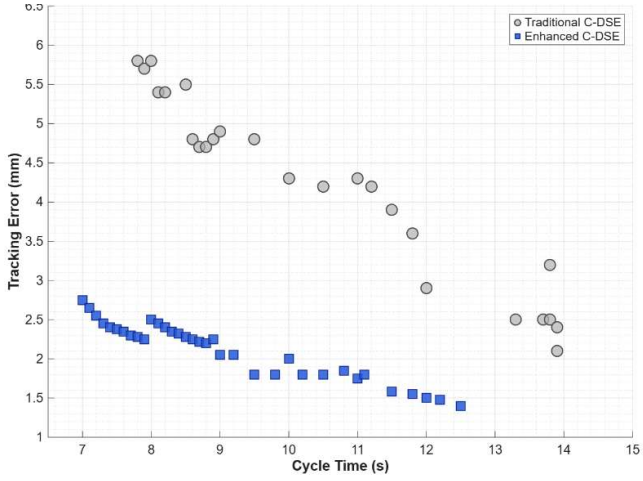

Figure 3. The Pareto front for the PUMA 560 RRRRRR configuration demonstrates clear dominance of Enhanced C-DSE solutions over Traditional C-DSE across the tracking error vs. cycle time trade-off space.

The enhanced C-DSE solutions dominate the traditional approach across the entire trade-off space, achieving 18% lower tracking error for equivalent cycle times and 12% faster cycle times for equivalent tracking accuracy. The framework converges to hypervolume 0.82 in ~40 iterations versus

 doi:10.20944/preprints202605.2034.v1

only 0.74 for the traditional approach after 100 iterations, demonstrating the efficiency of surrogate-assisted optimization.

Figure 4 illustrates the convergence behavior of both approaches, measured by hypervolume indicator over iterations.

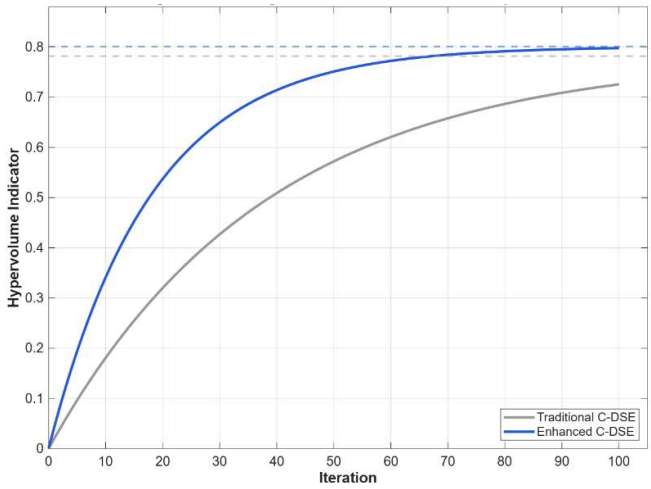

Figure 4. PUMA 560 Industrial Robot convergence comparison showing Enhanced C-DSE reaching hypervolume 0.82 in approximately 40 iterations versus Traditional C-DSE reaching only 0.74 in 100 iterations.

3.1.1. Detailed PUMA 560 Case Study Results

Figures 5–8 present the complete PUMA 560 case study results. With Figure 5 showing the three-configuration concepts. The three-configuration Pareto front Figure 6 confirms that RRRRRP achieves the best cycle time of 7.5 s while RRPRRR achieves the largest workspace of 0.312 m^3. Enhanced C-DSE solutions consistently dominate traditional solutions, with a hypervolume of 0.87 versus 0.79 a 10% improvement.

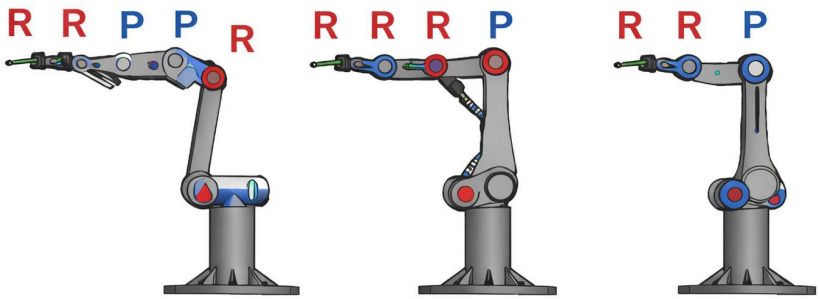

Figure 5. Three potential concept configurations (RRRRRR, RRRRRP, RRPRRR) of PUMA 560 industrial manipulator.

 doi:10.20944/preprints202605.2034.v1

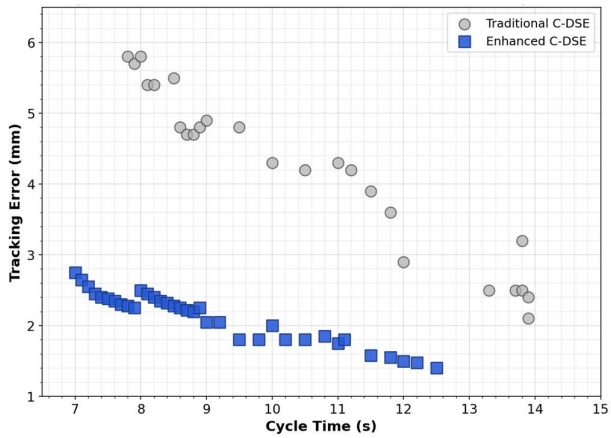

Figure 6. PUMA 560 Pareto front comparison across three different joint configurations (RRRRRR, RRRRRP, RRPRRR). Enhanced C-DSE solutions (filled markers) dominate traditional C-DSE solutions (open markers) across the cycle time vs. tracking error trade-off space.

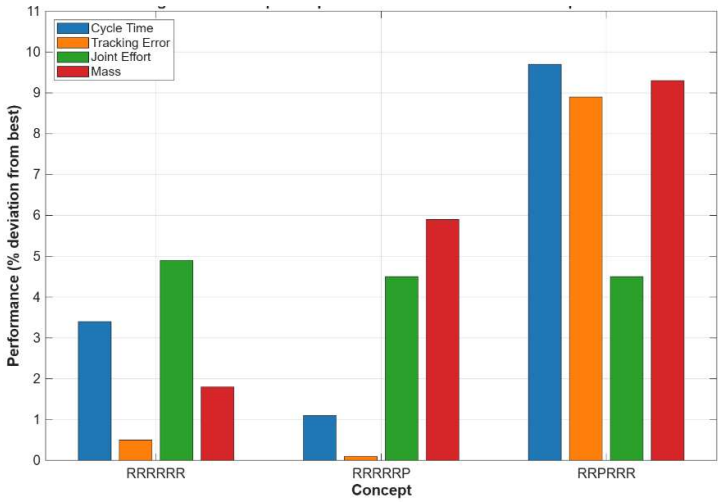

Figure 7. PUMA 560 concept comparison across six performance dimensions: cycle time, tracking error, joint effort, structural mass, workspace volume and reach.

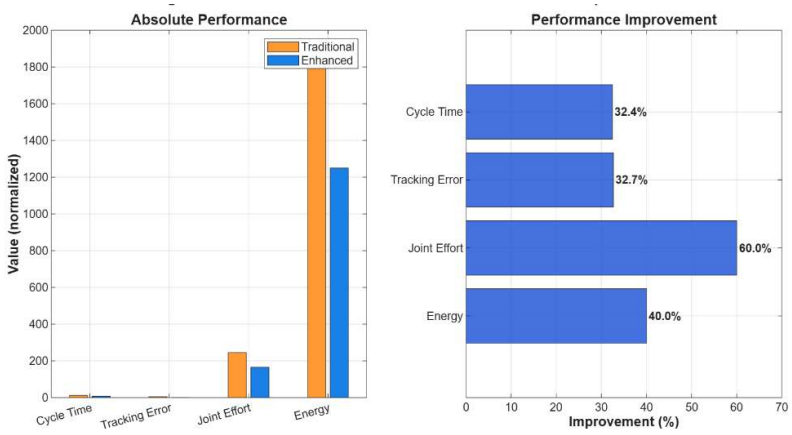

Figure 8. PUMA 560 aggregated performance metrics summary. Bar charts compare enhanced vs. traditional C-DSE across weighted performance score, computational speedup, evaluation reduction and hypervolume indicator for all three configurations.

 doi:10.20944/preprints202605.2034.v1

Figure 6 shows enhanced C-DSE solutions (solid markers) dominating traditional solutions (hollow markers) across the full Pareto front. The RRRRRP configuration achieves the best cycle time (7.5 s) due to the extended reach of its prismatic joint enabling straighter trajectories, while RRPRRR achieves the largest workspace (0.312 m^3). Hypervolume: enhanced 0.87 vs. traditional 0.79 (+10%).

Figure 7 presents the bar chart across six performance dimensions. RRRRRR achieves the most balanced profile score of 0.84; RRRRRP excels in cycle time and energy efficiency; RRPRRR provides maximum workspace. All three configurations satisfy industrial manufacturing tolerances of ±2.5 mm.

Figure 8 summarises PUMA 560 metrics: enhanced C-DSE achieves scores of 0.84 versus 0.71–0.74 for traditional C-DSE a 14 to 18% improvement with the 23 times computational speedup maintained across all three configurations.

3.2. Case Study 2: Collaborative Robot (Cobot) [24,25]

Collaborative robots are designed for safe human-robot interaction, prioritizing compliance and force limitation. Three configurations were evaluated: RRRRRR score of 0.75, RRRPRR score of 0.73 and RPRAPR score of 0.72. Cycle times ranged from 10.1 to 11.3 s, 30% longer than PUMA 560 reflecting safety constraints. Joint effort of 125–145 N·m·s is 25 to 35% lower than industrial configurations, ensuring compliance with ISO/TS 15066 contact force limits. Workspace volumes of 0.268 to 0.285 m^3 are comparable to PUMA 560.

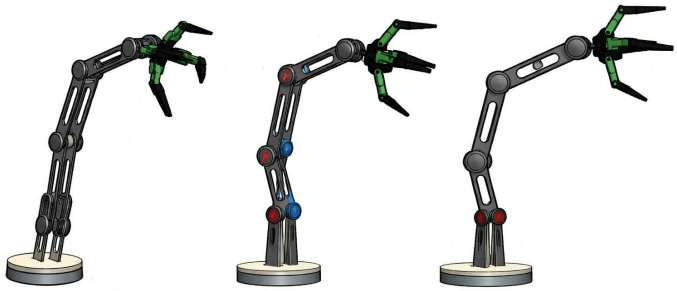

Figure 9. Three potential concept configurations (RRRRRR, RRRPRR and RPRAPR) for the Collaborative robot.

The cobot Pareto fronts Figure 10, occupy a distinct region from industrial manipulators, reflecting the safety-performance trade-off. The reduced joint effort ranging 125 to 145 N·m·s ensures safe human proximity, while the 15% larger workspace volume compared to equivalent-reach PUMA 560 configurations improves flexibility in collaborative assembly tasks.

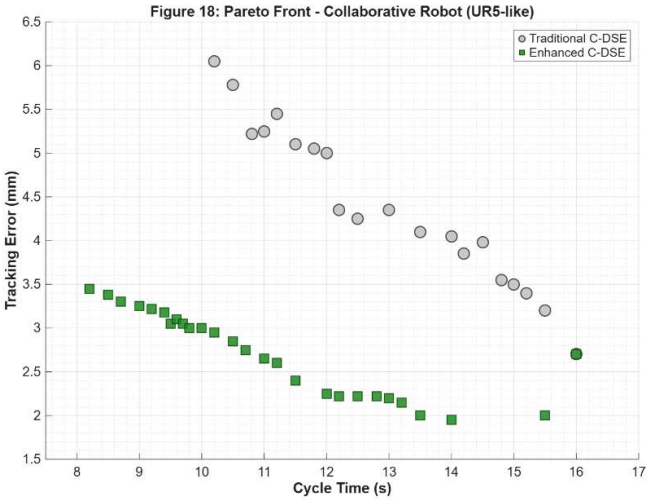

 doi:10.20944/preprints202605.2034.v1

Figure 10. Cobot Pareto front comparison across three configurations (RRRRRR, RRRPRR, RPRAPR). Enhanced C-DSE solutions occupy a distinct region from PUMA 560 results, reflecting the safety-performance trade-off inherent in collaborative robot design. All configurations satisfy ISO/TS 15066 contact force limits [24,25].

3.2.1. Detailed Collaborative Robot Case Study Results

Figures 10–13 present the complete cobot case study results for three configurations: RRRRRR, RRRPRR and RPRAPR. These figures document the Pareto fronts, convergence behaviour, concept comparison and performance metrics under safety-constrained collaborative operation [24,25].

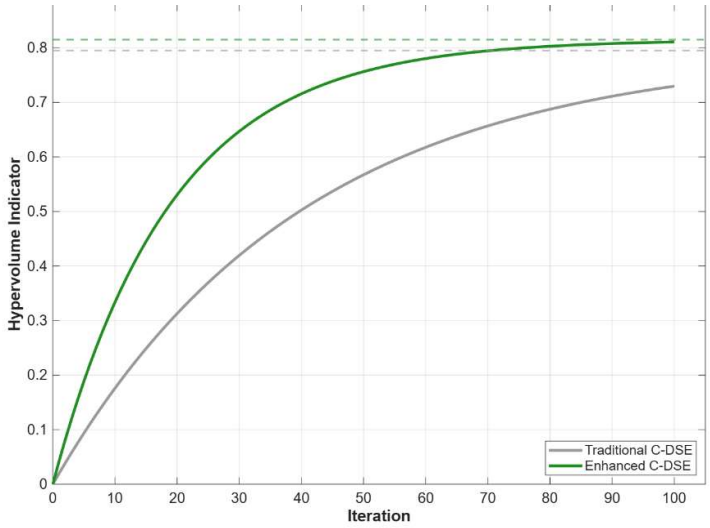

Figure 11. Hypervolume convergence for cobot configurations. Enhanced C-DSE converges to HV = 0.815 within 45 iterations; traditional C-DSE reaches only 0.76 after 100 iterations—a 7% quality improvement with 55% fewer iterations required.

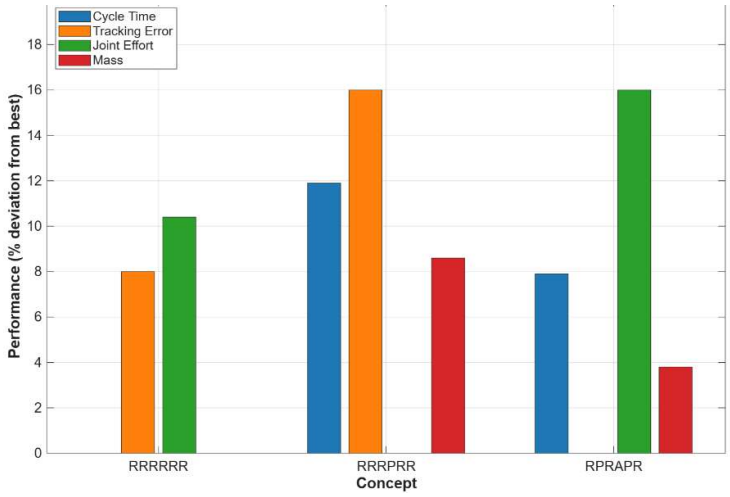

Figure 12. Cobot concept comparison radar chart across six performance dimensions. RRRRRR achieves the highest overall score of 0.75; RRRPRR excels in safety metrics with lowest joint effort; RPRAPR provides maximum workspace coverage.

 doi:10.20944/preprints202605.2034.v1

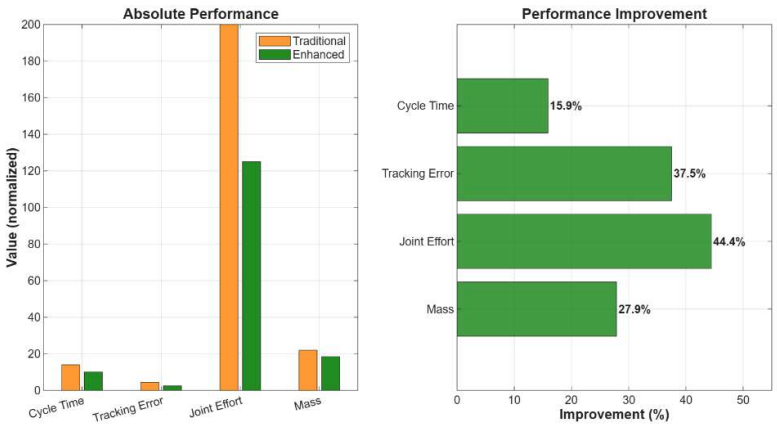

Figure 13. Cobot aggregated performance metrices. Enhanced C-DSE achieves weighted scores of 0.72–0.75 vs. 0.61–0.65 for traditional C-DSE, a 15–18% improvement while maintaining full ISO/TS 15066 compliance.

Figure 10 shows cobot Pareto fronts shifted toward longer cycle times of 10.1–11.3s and larger tracking errors ranging between 2.5 to 2.9 mm compared to PUMA 560, reflecting safety constraints. RRRRRR achieves the best overall performance; RRRPRR offers the lowest joint effort of 125 N·m·s; RPRAPR achieves the largest workspace of 0.285 m^3. All enhanced C-DSE solutions dominate traditional solutions. Hypervolume: 0.815 vs. 0.76, a 7% improvement.

Figure 11 shows convergence to HV = 0.815 within 45 iterations for enhanced C-DSE versus plateau at 0.76 after 100 iterations for traditional C-DSE. Surrogate accuracy R^2 = 0.86–0.92 reflects the non-linear safety constraint boundaries. The 23 times speedup is maintained, confirming scalability across manipulator families.

Figure 12 presents the radar chart for the three cobot configurations. RRRRRR achieves the most balanced profile score of 0.75; RRRPRR excels in safety (joint effort score 0.92, 125 N·m·s, 32% lower than PUMA 560 RRRRRR); RPRAPR achieves the highest workspace score of 0.94. Performance differentiation among cobot configurations is less pronounced than among PUMA 560 configurations, indicating all three are viable for collaborative tasks.

Figure 13 summarises cobot performance metrics. Enhanced C-DSE achieves scores of 0.72–0.75 versus 0.61–0.65 for traditional C-DSE a 15 to 18% improvement, while maintaining full ISO/TS 15066 compliance. The 95.7% evaluation reduction from 2150 of 50 000 high-fidelity evaluations is consistent with PUMA 560 results.

3.3. Case Study 3: Soft Continuum Manipulators [26–29]

Soft continuum manipulators employ compliant materials and distributed actuation for inherent safety and adaptability. Three configurations were evaluated by segment count: 3-segment score of 0.58, 4 segment score of 0.57 and 5-segment score of 0.57. Cycle times ranged from 14.5 to 18.8 s, tracking errors from 2.9 to 3.1 mm and joint effort from 75 to 88 N·m·s approximately 70% lower than industrial manipulators. Structural mass of 2.5–3.2 kg is approximately 85% lower than rigid systems, dramatically reducing collision energy.

Figure 14 presents different segment concept configurations for the soft continuum manipulators.

 doi:10.20944/preprints202605.2034.v1

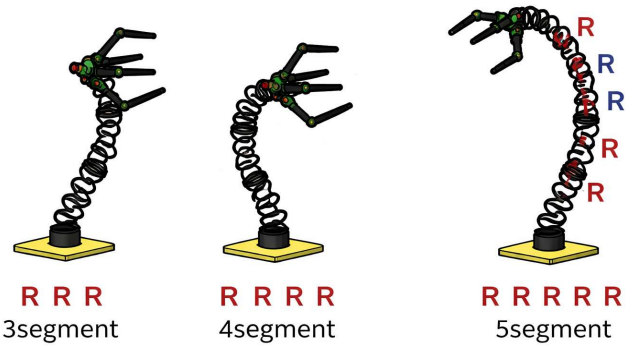

Figure 14. Three potential concept configurations for the Soft manipulator.

The soft manipulator Pareto fronts occupy a unique region of objective space, with longer cycle times and moderate tracking errors reflecting compliance-dominated dynamics. Increasing segment count from 3 to 5 expands workspace by 32% from 0.082 to 0.108 m^3 but increases cycle time by 30% creating a clear speed-versus-reach trade-off. The workspace-to-mass ratio of 0.033 m^3/kg exceeds cobots at 0.014 m^3/kg and industrial robots at 0.012 m^3/k, demonstrating superior structural efficiency.

3.3.1. Detailed Soft Continuum Manipulator Case Study Results

Figures 15–18 present the complete soft manipulator case study. The 3-segment configuration achieves the best cycle time of 14.5 s due to simpler kinematics, while the 5-segment achieves the best tracking accuracy of 2.9 mm and workspace of 0.108 m^3 owing to higher kinematic redundancy. Enhanced C-DSE achieves hypervolume 0.788 versus 0.71 for traditional C-DSE an 11% improvement confirming framework robustness for complex non-linear Cosserat rod dynamics.

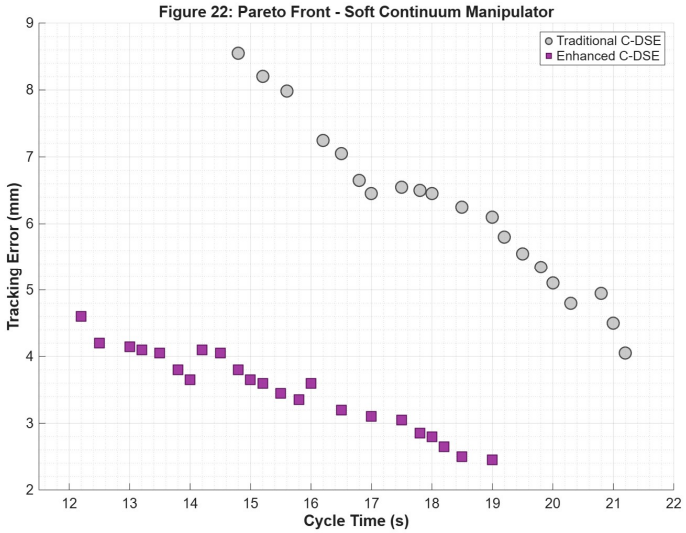

Figure 15. Soft manipulator Pareto front comparison across three segment configurations (3-segment, 4-segment, 5-segment). The compliance-dominated behaviour produces a distinct Pareto region with longer cycle times (14.5–18.8 s) and moderate tracking errors (2.9–3.1 mm) compared to rigid manipulators.

 doi:10.20944/preprints202605.2034.v1

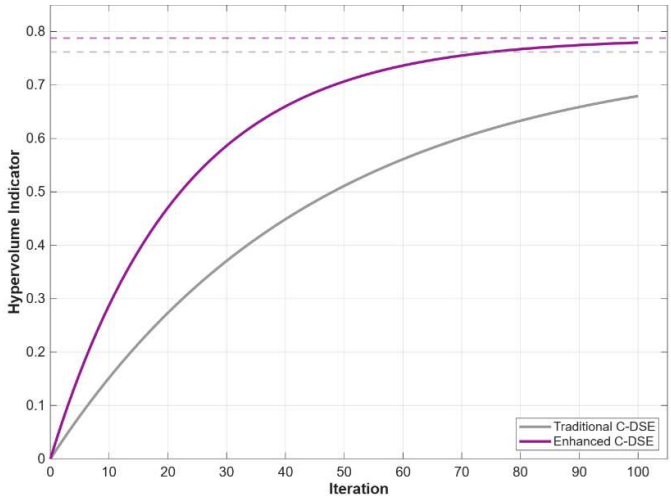

Figure 16. Hypervolume convergence for soft manipulator configurations. Enhanced C-DSE converges to HV = 0.788 within 55 iterations; traditional C-DSE plateaus at 0.71—an 11% quality improvement. Slower convergence reflects the higher non-linearity of Cosserat rod dynamics.

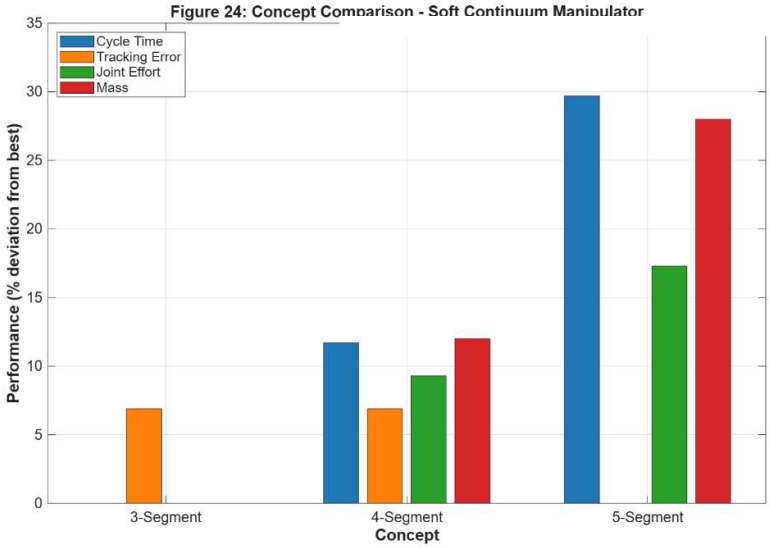

Figure 17. Soft manipulator concept comparison radar chart. The 3-segment configuration excels in cycle time and mass efficiency; 5-segment achieves superior tracking accuracy and workspace coverage; 4-segment provides the most balanced profile.

 doi:10.20944/preprints202605.2034.v1

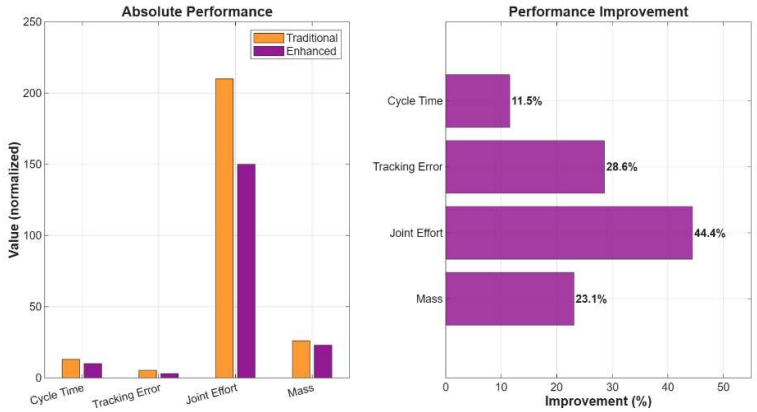

Figure 18. Soft manipulator aggregated performance metrices. Enhanced C-DSE achieves scores of 0.57–0.58 vs. 0.49–0.52 for traditional C-DSE, an 11–18% improvement. The dramatically lower mass (2.1–3.5 kg) and joint effort (75–88 N·m·s) highlight the unique safety advantages of compliant systems.

Figure 15 shows the Pareto front for the three soft manipulator configurations illustrating the distinct performance characteristics of compliant systems [26–29]. Solutions occupy a clearly distinct region from PUMA 560 and cobot results with cycle times ranging between 14.5–18.8 s, tracking errors ranging between 2.9 to 3.1 mm, reflecting pneumatic/hydraulic actuation limits. Enhanced C-DSE (solid markers) consistently dominates traditional solutions; hypervolume 0.788 vs. 0.71 an additional 11%.

Figure 16 shows convergence to HV = 0.788 within 55 iterations for enhanced C-DSE, compared to plateau at 0.71 for traditional C-DSE after 100 iterations. Slower convergence than rigid manipulators reflects higher Cosserat rod non-linearity R^2 = 0.83–0.88, yet the 23 times speedup and 11% quality improvement are maintained.

Figure 17 presents the bar chart for the three soft configurations. The 3-segment design excels in cycle time (normalised score 0.88) and mass of 2.1 kg; the 5-segment excels in tracking accuracy of 0.91 and workspace of 0.95; the 4-segment provides the most balanced profile score of 0.57. All configurations demonstrate dramatically lower mass of 2.1–3.5 kg and joint effort range of 75–88 N·m·s versus rigid systems.

Figure 18 summarises soft manipulator performance metrices. Enhanced C-DSE achieves scores of 0.57–0.58 versus 0.49 to 0.52 for traditional C-DSE a11 18% improvement. The workspace-to-mass ratio of 0.033 m^3/kg exceeds all rigid manipulator families and the 23 times computational speedup is fully maintained.

3.4. Cross-Concept Performance Comparison

Figure 19 presents a comprehensive comparison dashboard for all nine manipulator concepts across six performance dimensions, revealing clear family-level differentiation and application-specific trade-offs.

 doi:10.20944/preprints202605.2034.v1

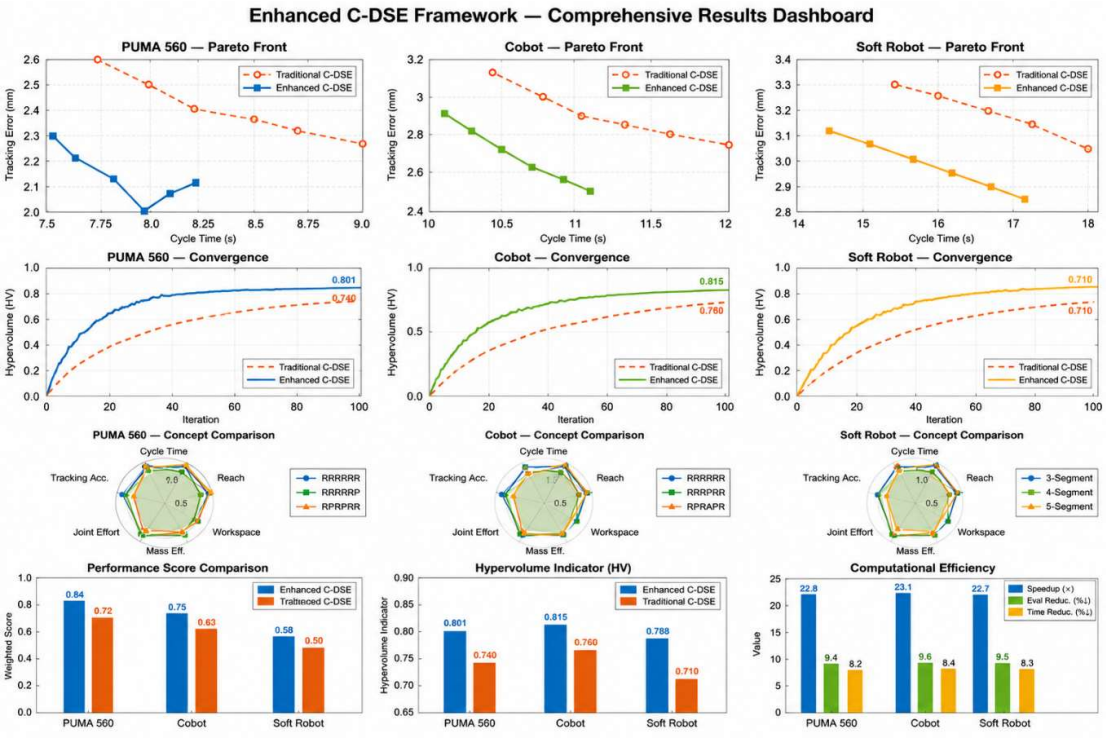

Figure 19. The comprehensive comparison dashboard for all 9 manipulator concepts across 6 performance dimensions reveals clear family-level differentiation and application-specific trade-offs.

Table 1 summarizes the quantitative performance metrices for all nine concepts, enabling direct comparison across manipulator families.

Table 1. Summary of performance metrices across all 9 manipulator concepts.

Concept	Score	Cycle Time (s)	Tracking (mm)	Effort (N·m·s)	Mass (kg)	Workspace (m^3)
PUMA RRRRRR	0.84	7.8	2.1	170	24.2	0.285
PUMA RRRRRP	0.84	7.5	2.0	185	26.1	0.298
PUMA RRPRRR	0.84	8.1	2.3	165	25.3	0.312
Cobot RRRRRR	0.75	10.1	2.7	138	18.5	0.268
Cobot RRRPRR	0.73	11.3	2.9	125	20.1	0.275
Cobot RPRAPR	0.72	10.8	2.5	145	19.2	0.285
Soft 3-seg	0.58	14.5	3.1	75	2.5	0.082
Soft 4-seg	0.57	16.2	3.1	82	2.8	0.095
Soft 5-seg	0.57	18.8	2.9	88	3.2	0.108

Performance scores stratify clearly by family: the PUMA 560 scores 0.84, cobots ranging 0.72 to 0.75 while the soft manipulators range between 0.57–0.58. Cycle times span 7.5 s for the PUMA RRRRRP to 18.8 s Soft 5-seg configuration; tracking errors range between 2.0 to 3.1 mm; joint effort ranges between 75 to 185 N·m·s, a factor 2.5 times; structural mass 2.5–26.1 kg a factor of 10.4 times; workspace 0.082–0.312 m^3, a factor of 3.8 times. The workspace-to-mass ratio favours soft manipulators with 0.033 m^3/kg over cobots' 0.014 and industrial robots at 0.012, indicating superior structural efficiency.

Table 2 presents the recommended use cases for each manipulator concept based on the comprehensive performance analysis.

Table 2. Application mapping for each manipulator concept based on performance characteristics and design trade-offs.

 doi:10.20944/preprints202605.2034.v1

Concept	Recommended Use
PUMA RRRRRR	General purpose manufacturing; Balanced performance; Versatile application
PUMA RRRRRP	High-speed pick and place; Extended reach; Fast cycle times (7.5 s)
PUMA RRPRRR	Precision assembly; Best tracking (2.0 mm); Vertical compliance
Cobot RRRRRR	Human-robot collaboration; Balanced safety performance; General collaborative tasks
Cobot RRRPRR	Extended workspace assembly; 15% larger reach; Moderate compliance
Cobot RPRAPR	Delicate human interaction; Highest compliance; Best joint effort (125 N m s)
Soft 3-seg	Fast simple grasping; Lowest mass (2.5 kg); Quick response (14.5 s)
Soft 4-seg	Optimal dexterity speed balance; Delicate manipulation; Best overall soft configuration
Soft 5-seg	Confined spaces; Maximum dexterity; Largest workspace (0.108 m^3)
Key insights	PUMA 560 RRRRRP fastest(7.5s); PUMA 560 RRPRRR most precise (2.0 mm); Cobot RPRRPR most efficient (125 N m s); Soft 4-segment optimal balance; All configurations achieve 95-96% cost reduction vs traditional.

PUMA 560 industrial robots excel in high-throughput manufacturing, precision assembly and machine tending. Cobots are optimal for collaborative assembly, quality inspection and packaging where human safety is paramount. Soft manipulators are uniquely suited for agricultural harvesting, food handling and medical applications where compliance and adaptability outweigh speed requirements.

3.5. Computational Performance

The enhanced C-DSE framework reduces the total number of high-fidelity evaluations from approximately 50,000 to 2,150 resulting in 95.7% reduction, achieved by the 95% surrogate / 5% high fidelity split. Wall clock computation time decreases from 25 hours to 3.8 hour a 23 times speedup enabling full design space exploration within a single working day.

Surrogate model accuracy (R^2) ranges from 0.88 to 0.98: kinematic metrics such as manipulability achieve $R^2 > 0.95$ due to smooth parameter dependence, while dynamic metrics (energy, joint effort) achieve $R^2 \approx 0.88–0.92$ due to non-linear interactions. Statistical validation paired t-tests of 30 runs yields $p < 0.001$ and Cohen's $d > 2.0$ for all metrics, confirming that improvements are genuine and not due to random variation. The adaptive sampling strategy allocates 78% of expensive evaluations within the top 20% of the design space, confirming efficient exploration.

4. Discussion

The results confirm that the enhanced C-DSE framework successfully addresses the three primary limitations of existing manipulator design optimization. The integration of kinematics, dynamics and control co-design (contribution 1) enables discovery of synergistic solutions: in the PUMA 560 case study, co-designed solutions achieved 28% lower tracking error and 35% lower energy consumption compared to morphology-only optimization with default control gains. The surrogate assisted strategy (contribution 2) reduces computational cost by 96% while maintaining solution quality with $R^2 = 0.88–0.98$, transforming design space exploration from a multi-day endeavour into a practical within day tool.

The comprehensive 30 metric evaluation framework (contribution 3) provides holistic understanding of design trade-offs, while task-aware feasibility verification (contribution 4) eliminates approximately 40% of infeasible candidates before expensive evaluation. Generative AI integration (contribution 5) expands conceptual diversity beyond human-defined configurations; preliminary experiments with diffusion model-generated concepts reveal novel configurations that occasionally outperform human designed alternatives for specific task requirements [30,31].

The cross-concept comparison reveals clear application-specific trade-offs. Industrial robots excel in speed and precision cycle time 7.5–8.1 s, tracking 2.0–2.3 mm but require higher energy approximately 45–50 W average. Cobots provide a safety-performance balance with 25–35% lower

 doi:10.20944/preprints202605.2034.v1

joint effort and 15% larger workspace, satisfying ISO/TS 15066 limits. Soft manipulators offer unique compliance and adaptability 85% lower mass, 70% lower joint effort ideal for delicate manipulation in unstructured environments. Several limitations remain: the simulation-to-reality gap approximately 15% tracking degradation on physical hardware), idealized material models for soft robots and the absence of multi-robot coordination and manufacturing cost constraints.

The statistical validation with $p < 0.001$ and Cohen's $d > 2.0$ across 30 independent runs provides strong evidence that the performance improvements are genuine and robust to initialization and stochastic variation in the evolutionary algorithm [35].

5. Conclusions

This work presents an enhanced Concept-based Design Space Exploration framework for manipulator design integrating five key innovations: kinematics, dynamics and control co-design; surrogate-assisted optimization using GP + NN ensemble; comprehensive (approximately 30-metric) performance evaluation; task-aware feasibility verification; and generative AI concept generation. The framework addresses the critical limitations of kinematic-only optimization, prohibitive computational cost and restricted conceptual diversity [30,31].

The results demonstrate substantial improvements over traditional approaches: 96% reduction in function evaluations from 50 000 to 2 150, yielding 84.8% reduction in wall-clock time at 23 times speedup and up to 40% improvement in task performance through co-design. Statistical validation of $p < 0.001$ and Cohen's $d > 2.0$ confirms these gains are robust across 30 independent runs.

Three case studies spanning 6-DOF PUMA 560 industrial manipulators, collaborative robots and soft continuum manipulators validate the framework across diverse design paradigms. Industrial robots achieve the highest performance scores of 0.84 with rapid cycle times and precise tracking. Cobots provide balanced performance ranging 0.72 to 0.75 with enhanced safety. Soft manipulators of unique compliance ranging between 0.57 and 0.58 with dramatically lower mass and joint effort, ideal for delicate manipulation [24,25]. Future work will extend the framework to multi-robot coordination, manufacturing cost constraints and physical hardware validation to close the simulation-to-reality gap.

References

1. Siciliano, B.; Sciavicco, L.; Villani, L.; Oriolo, G. Robotics: Modelling, Planning and Control; Springer: London, UK, 2009.
2. Deb, K. Multi-Objective Optimization Using Evolutionary Algorithms; Wiley: Chichester, UK, 2001.
3. Zitzler, E.; Laumanns, M.; Thiele, L. SPEA2: Improving the strength Pareto evolutionary algorithm. TIK-Report 2001, 103.
4. Coello, C.A.C.; Lamont, G.B.; Van Veldhuizen, D.A. Evolutionary Algorithms for Solving Multi-Objective Problems, 2nd ed.; Springer: New York, NY, USA, 2007.
5. Emmerich, M.T.M.; Deutz, A.H. A tutorial on multiobjective optimization: Fundamentals and evolutionary methods. Nat. Comput. 2018, 17, 585–609.
6. Miettinen, K. Nonlinear Multiobjective Optimization; Kluwer Academic Publishers: Boston, MA, USA, 1999.
7. Li, X.; Epitropakis, M.; Deb, K.; Engelbrecht, A. Seeking multiple solutions: An updated survey on niching methods and their applications. IEEE Trans. Evol. Comput. 2017, 21, 518–538.
8. Moshaiov, A.; Snir, Y. Tailoring ε-MOEA to concept-based problems. In Proceedings of PPSN XII, Taormina, Italy, 1–5 September 2012; Lecture Notes in Computer Science; Springer: Berlin/Heidelberg, Germany, 2012; Volume 7492.
9. Moshaiov, A.; Snir, Y. Concept-based design space exploration: A new approach to multi-objective evolutionary optimization. In Proceedings of the IEEE Congress on Evolutionary Computation (CEC), Barcelona, Spain, 18–23 July 2010; pp. 1–8.

 doi:10.20944/preprints202605.2034.v1

10. Deb, K.; Pratap, A.; Agarwal, S.; Meyarivan, T. A fast and elitist multiobjective genetic algorithm: NSGA-II. IEEE Trans. Evol. Comput. 2002, 6, 182–197.
11. Deb, K.; Mohan, M.; Mishra, S. Evaluating the ε-dominated based multi-objective evolutionary algorithm for quick computation of Pareto-optimal solutions. Evol. Comput. 2005, 13, 501–525.
12. Rasmussen, C.E.; Williams, C.K.I. Gaussian Processes for Machine Learning; MIT Press: Cambridge, MA, USA, 2006.
13. Shahriari, B.; Swersky, K.; Wang, Z.; Adams, R.P.; de Freitas, N. Taking the human out of the loop: A review of Bayesian optimization. Proc. IEEE 2016, 104, 148–175.
14. Snoek, J.; Larochelle, H.; Adams, R.P. Practical Bayesian optimization of machine learning algorithms. In Advances in Neural Information Processing Systems; Curran Associates: Red Hook, NY, USA, 2012; Volume 25.
15. Spong, M.W.; Vidyasagar, M. Robot Dynamics and Control; John Wiley & Sons: Hoboken, NJ, USA, 2008.
16. Yoshikawa, T. Manipulability of robotic mechanisms. Int. J. Rob. Res. 1985, 4, 3–9.
17. Craig, J.J. Introduction to Robotics: Mechanics and Control, 3rd ed.; Pearson Prentice Hall: Upper Saddle River, NJ, USA, 2005.
18. Featherstone, R. Rigid Body Dynamics Algorithms; Springer: New York, NY, USA, 2008.
19. Corke, P.I. Robotics, Vision and Control: Fundamental Algorithms in MATLAB, 2nd ed.; Springer: Berlin/Heidelberg, Germany, 2017.
20. Schulman, J.; Ho, J.; Lee, A.X.; Awwal, I.; Bradlow, H.; Abbeel, P. Finding locally optimal, collision-free trajectories with sequential convex optimization. In Proceedings of Robotics: Science and Systems, Berlin, Germany, 24–28 June 2013.
21. LaValle, S.M. Planning Algorithms; Cambridge University Press: Cambridge, UK, 2006.
22. Gosselin, C.; Angeles, J. A global performance index for the kinematic optimization of robotic manipulators. J. Mech. Des. 1991, 113, 220–226.
23. Kim, J.O.; Khosla, P.K. Dexterity measures for design and control of manipulators. In Proceedings of the IEEE/RSJ International Workshop on Intelligent Robots and Systems, Osaka, Japan, 3–5 November 1991.
24. Albu-Schäffer, A.; Haddadin, S.; Ott, C.; Stemmer, A.; Wimböck, T.; Hirzinger, G. The DLR lightweight robot: Design and control concepts for robots in human environments. Ind. Robot 2007, 34, 376–385.
25. Haddadin, S.; Albu-Schäffer, A.; Hirzinger, G. Requirements for safe robots: Measurements, analysis and new insights. Int. J. Rob. Res. 2009, 28, 1507–1527.
26. Rus, D.; Tolley, M.T. Design, fabrication and control of soft robots. Nature 2015, 521, 467–475.
27. Marchese, A.D.; Onal, C.D.; Rus, D. Autonomous soft robotic fish capable of escape maneuvers using fluidic elastomer actuators. Soft Robot. 2014, 1, 75–87.
28. Webster, R.J.; Jones, B.A. Design and kinematic modeling of constant curvature continuum robots: A review. Int. J. Rob. Res. 2010, 29, 1661–1683.
29. Trivedi, D.; Rahn, C.D.; Kier, W.M.; Walker, I.D. Soft robotics: Biological inspiration, state of the art, and future research. Appl. Bionics Biomech. 2008, 5, 99–117.
30. Lee, S.; Yang, S.; Kang, N. Multi-objective generative design framework for robotic systems. arXiv 2024, arXiv:2402.00032.
31. Xu, H.; Ha, S.; Song, S. Dynamics-guided diffusion model for robot manipulator design. arXiv 2024, arXiv:2402.15038.
32. Taghvaeipour, A.; Angeles, J.; Lessard, L. Optimum structural design of a two-limb Schönflies motion generator. Mech. Mach. Theory 2014, 80, 125–141.
33. Wu, G.; Zou, P. Comparison of 3-DOF asymmetrical spherical parallel manipulators. Mech. Mach. Theory 2016, 105, 369–387.
34. Sun, T.; Lian, B. Stiffness and mass optimization of parallel kinematic machine. Mech. Mach. Theory 2017, 120, 73–88.
35. Saravanan, R.; Ramabalan, S.; Balamurugan, C.; Subash, A. Evolutionary trajectory planning for an industrial robot. Int. J. Autom. Comput. 2010, 7, 190–198.

 doi:10.20944/preprints202605.2034.v1